


How to Characterize Emerging Luminescent Semiconductors with Unknown Photophysical Properties

Alan R. Bowman^{1,†} and Samuel D. Stranks^{1,2,*}

¹*Cavendish Laboratory, Department of Physics, University of Cambridge, J.J. Thomson Avenue, Cambridge CB3 0HE, United Kingdom*

²*Department of Chemical Engineering & Biotechnology, University of Cambridge, Philippa Fawcett Drive, Cambridge CB3 0AS, United Kingdom*

 (Received 19 December 2022; revised 17 April 2023; published 20 June 2023)

Luminescent semiconductors are the key material in a host of optoelectronic devices, including solar cells, light-emitting diodes, and x-ray scintillators, and have been discovered at an increasing rate over the last decades. To optimize any device, a luminescent semiconductor's photophysics must be understood and its loss processes minimized. Several accessible spectroscopic techniques exist, which can together give all relevant photophysical information, namely, UV-Vis spectroscopy, photoluminescence quantum efficiency, and time-resolved photoluminescence. However, these measurements are often poorly used, incorrectly fitted, or important information is missed. Here, we present best practices in applying these techniques to characterize luminescent semiconductors with unknown photophysical properties. We highlight which information can be obtained from each measurement, when it is appropriate to apply different mathematical models, and give examples from a range of semiconductors. This work will help to standardize and streamline the characterization of luminescent semiconductors, enabling more efficient devices.

DOI: [10.1103/PRXEnergy.2.022001](https://doi.org/10.1103/PRXEnergy.2.022001)

CONTENTS

I. INTRODUCTION	1
II. ABSORPTION	3
III. PHOTOLUMINESCENCE	3
IV. ABSORPTION AND PHOTOLUMINESCENCE SHAPE	5
V. PHOTOLUMINESCENCE QUANTUM EFFICIENCY (PLQE)	5
VI. TIME-RESOLVED PHOTOLUMINESCENCE (TRPL)	6
VII. TRANSLATION TO DEVICES	9
VIII. CONCLUSION	10
ACKNOWLEDGMENTS	10
REFERENCES	10

I. INTRODUCTION

Luminescent semiconductors are being developed for a host of optoelectronic applications, including solar cells, light-emitting diodes, and x-ray scintillators [1–3]. Promising material families being researched significantly include halide perovskite, bismuth-based, and organic semiconductors [4–6]. Understanding the nature of excited states in these materials—whether they are excitonic (bound electrons and holes) or free charge like, how much energy loss occurs before radiative recombination, and identifying intrinsic material properties—is key to minimizing nonradiative processes and realizing high-quality devices.

In any semiconductor, excited species are generated following the absorption of light. Here, we define a semiconductor to be a material that absorbs photons above a band gap, with the band gap being useful for the desired application. Species excited in a semiconductor can include free electrons and holes, excitons, filled traps (both surface and bulk), phonons, and polarons. An experimenter's aim is to identify the simplest physical model that explains all observations. For example, bulk GaAs at room temperature is described as having rapidly diffusing free electrons and holes: while exciton formation must occur within the material typically this process is not necessary to explain spectroscopic data [7].

*sds65@cam.ac.uk

†Current address: Laboratory of Nanoscience for Energy Technologies, EPFL, MED 1 2526 (Bâtiment MED), Station 9, CH-1015 Lausanne, Switzerland.

Published by the American Physical Society under the terms of the [Creative Commons Attribution 4.0 International](https://creativecommons.org/licenses/by/4.0/) license. Further distribution of this work must maintain attribution to the author(s) and the published article's title, journal citation, and DOI.

A host of advanced optical techniques exist to characterize materials, including ultrafast transient absorption and terahertz spectroscopy. However, most laboratories only have access to more generalized equipment, namely, UV-vis spectroscopy, photoluminescence (PL), photoluminescence quantum efficiency (PLQE), and time-resolved photoluminescence (TRPL) [8,9]. These simpler techniques are extremely powerful tools, which, when applied correctly, can reveal similar levels of information about semiconductors to more advanced experiments. We restrict our text to fully optical measurements, though we note that other accessible measurements, for example, photoconductivity, can also provide important information.

Here, we discuss how to characterize new luminescent semiconductors with readily available experimental apparatus and no prior material knowledge to identify a reasonable model. We present examples from a range of semiconductor material families that have varied spectroscopic behaviors. Our only assumptions are that material properties are sufficiently homogeneous across the illuminated region for these techniques to be applicable (i.e., lateral carrier diffusion and local sample heterogeneity can be ignored, or measurements are done on a macroscopic single crystal) and that the sample is either free standing or deposited on, or encapsulated between, glass or other spectroscopically and electronically passive materials; we discuss the case of full device stacks in Sec. VII. We emphasize that measurement repeatability (including on samples fabricated in different batches and on different spots on the sample) and measuring the spectroscopic and electronic reference characteristics of substrates is key for rigorous characterization of a semiconductor. These guidelines will enable rigorous characterization and rapid sample screening (when compared to, for example, pump-probe measurements), allowing for deficiencies in material properties to be identified, the types of excited species present within their material to be understood, and initial quantifications of sample stability to be made. Adoption of such approaches will increase the speed and development of the next generation of luminescent semiconductor-based devices for a variety of applications.

Excitations are generated in a semiconductor following the absorption of photons. Excitations typically fall into two broad categories: excitonic, where excited electrons and holes are strongly bound to each other, and free charges, which can travel separately within a material [Figs. 1(a) and 1(b)]. Ultimately excited electrons and holes will recombine, returning the semiconductor to an unexcited state. There are a wide range of processes that can lead to recombination. We briefly introduce the most common processes here (for free charges), to give the reader a clearer idea of processes that can be considered. Several excellent review papers and textbooks discuss these processes in more detail [11–13].

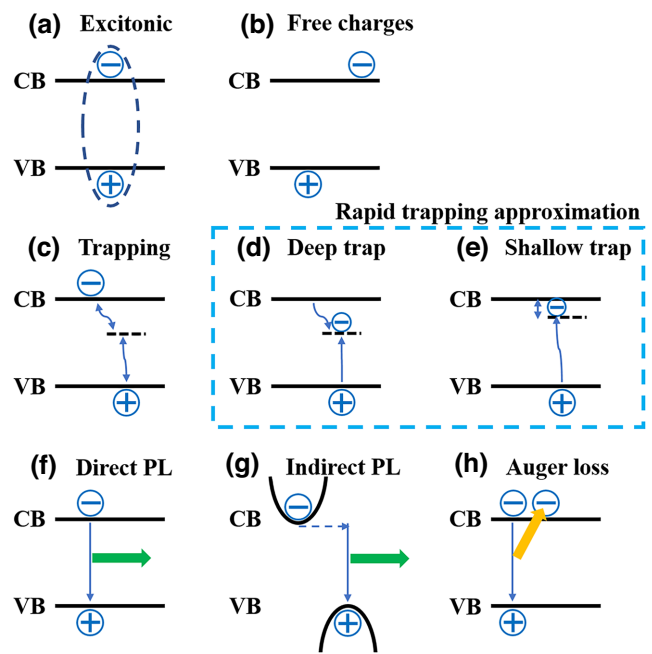


FIG. 1. (a),(b) Schematics of excitonic (i.e., bound) and free charges, respectively. (c) Typical picture for charge traps, with deep and shallow trap processes within the rapid trapping approximation (see the Supplemental Material Note 1 for definitions [10]) shown in (d),(e). (f),(g) Direct and phonon-mediated photoluminescence, respectively, and (h) Auger recombination. Here, VB and CB correspond to valence and conduction bands, respectively. In all plots, blue arrows show the change in energy level of an excited electron or hole, green arrows show photons, dashed blue arrows show phonons, and yellow arrow shows energy transfer from one excitation to a second.

Material imperfections result in trap-based recombination, which is commonly observed in semiconductors. A trap is an electronic state between the valence and conduction bands of a semiconductor (typically related to defects), which excitations can transition into and out of [Fig. 1(c)]. In nearly all trap models, rapid trapping is assumed, where traps are populated rapidly compared to the lifetime of excited charges (if this did not happen, then traps would not significantly affect the semiconductor). For traps that are energetically far from the conduction and valence bands, termed deep traps, it is typical for one excited carrier to become rapidly stuck at this energy level, and then the second excited charge carrier recombines with this filled trap at some subsequent time [Fig. 1(d)]. This is a first-order process, which depends on the concentration of charges in only the valence or conduction band. Conversely, for shallow traps close to the valence or conduction band, excited charges can rapidly transition between trap states and the conduction or valence bands. Therefore, for recombination to occur via a shallow trap, it requires the trap to be populated by both excited charges at the same time, meaning shallow trap recombination depends on the concentration of both excited electrons and

excited holes [Fig. 1(e)]. Other key recombination mechanisms are direct and phonon-mediated photoluminescence [Figs. 1(f) and 1(g)] and Auger recombination, where the energy from a recombination process is directly transferred to another excited charge carrier [instead of to phonons or photons, Fig. 1(h)].

From an experimental point of view, absorption measurements can provide significant information on the type of charge initially formed within the material and key information on the band structure. Photoluminescence and time-resolved measurements give details regarding different recombination processes and the timescales for energy loss. We now discuss the best approach to apply each measurement in turn.

II. ABSORPTION

Absorption measurements record sample reflection (R) and transmission (T) (for example, via UV-vis spectroscopy). This can either be done with the sample in free space, where only the direct transmission (reflection) spectra are recorded, or with the sample placed at the back (front) of an integrating sphere, which records the direct and diffuse reflection (transmission). In both cases, for comparison with experiments and theory, it is best practice to place the sample perpendicular to the incident beam and, for single-crystal samples, polarized measurements should also be considered (in the case of dichroism). When considering photonic or other anisotropic properties, exploring different angles of incidence may also be important. Diffuse values can be converted into sample absorption or absorptance, via $1-R-T$ (assuming R and T include all scattering contributions). Notably, this measurement requires only a white light source, an integrating sphere, a diffraction grating, and a detector, and only absolute wavelength calibration and relative intensity calibration are necessary (via a reference sample with known spectral response [14]).

Absorptance is a convolution of the sample's absorption, thickness, and surface roughness. Typically, it is difficult to quantify the exact relationship between these values and absorptance, except for materials with flat surfaces [15,16]. For flat films, it is possible to extract the absorption coefficient and gain significant information on thin-film interference effects, especially if samples of different thicknesses are measured. We note that the absorption coefficient is an intrinsic material property that can also be accessed by first-principles modeling (via joint density of electronic states [17]), so determination of its value can be extremely useful for theory-experiment comparison [18].

Tauc plotting can be used to measure the band gap of the material from its absorptance, with an outline of the technique, including its relation to a semiconductor's band structure, given in the Supplemental Material Note 2 [10,19]. The mathematical form of a Tauc fit is different

for direct-indirect band gaps and allowed-forbidden optical transitions. We present Tauc fitting for direct (GaAs) and indirect (silicon) band gap materials in Fig. 1(a), where the mathematical form of a Tauc plot is different in these cases. While, in principle, the direct-indirect comparison can be used to identify the kind of material being measured, care must be taken as both direct and indirect Tauc plotting can sometimes fit data well. We present this for a low-band-gap halide perovskite (direct band gap) sample in Fig. 2(a). Temperature measurements can play a role here, as near the band edge, indirect-band-gap materials require a phonon to proceed (so their absorption strength is reduced at low temperatures). Care must also be taken to avoid applying Tauc fitting to below-band-gap defect states, termed Urbach tails. Urbach tails can be fitted by an exponential decay in energy, providing information on the defect states in a material, while their functional form of an exponential decay allows an experimenter to differentiate between these and the semiconductor band gap [27]. Additionally, extreme care is needed if there is an exciton resonance peak at the band gap, as this requires the application of Elliot theory [28]. Further discussion of Tauc fitting can be found elsewhere [29]. One should aspire to determine the band gap as precisely as possible, for example, within 10 meV, but, even if this is not possible, Tauc fits give good estimations of the sample's band gap. If an integrating sphere is not available, Tauc fitting can still be applied to $1-T$ even for direct transmission, assuming that scattering and reflection contributions do not change in shape significantly around the band gap. The only additional correction is that the value of $1-T$ well below the band gap should be subtracted from all data, which removes arbitrary offsets. While Tauc plots estimate the band gap, performing Tauc fitting on external quantum efficiency measurements of full devices is a more meaningful approach to characterize extracted charges [30]. We discuss absorption shape further in Sec. IV.

III. PHOTOLUMINESCENCE

Here, a sample is excited by monochromatic light and the emission, as a function of wavelength, is recorded. Typically, the signal is recorded by a spectrometer. Wavelength and relative intensity (radiometric) calibration are always necessary prior to reporting results. This can be carried out via calibration lamps with well-known wavelength (e.g., mercury-argon) and emissivity (e.g., calibrated tungsten halogen lamps) calibration. Absolute radiometric calibration is not always necessary but can provide information regarding absolute luminescence efficiencies [31]. The shape of the photoluminescence is a function of the ground-state band structure; changes to the band structure prior to photon emission (e.g., via molecular reorganization from excited state-lattice coupling); sample temperature (i.e., coupling of electronic states to

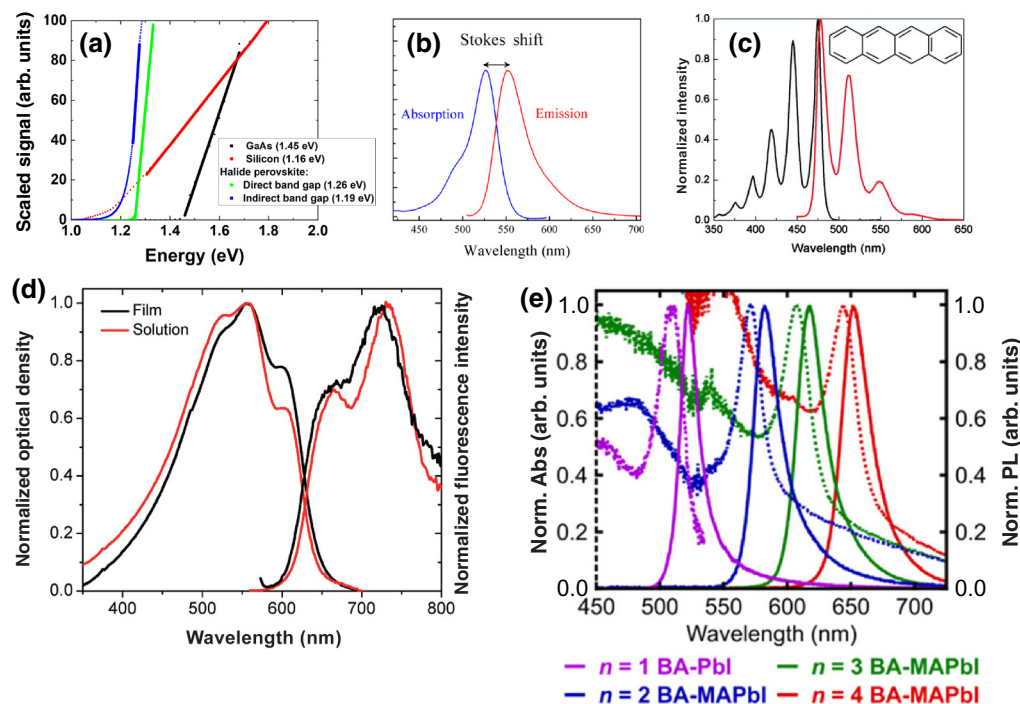


FIG. 2. (a) Tauc fit plots for GaAs (direct-band-gap Tauc model), silicon (indirect-band-gap Tauc model), and two fits for a low-band-gap halide perovskite (formamidinium lead tin iodide, FAPb_{0.5}Sn_{0.5}I₃) using direct- and indirect-band-gap Tauc models. Extracted band gaps obtained are marked on the legend. Data are scaled appropriately, so they all lie on the same plot, but we note the y axis is scaled differently for direct- and indirect-band-gap materials (see the Supplemental Material Note 2 [10]). This plot is generated using data from Papatryfonos *et al.* [20], Green [21], and Bowman *et al.* [22] for GaAs, silicon, and low-band-gap halide perovskite, respectively. (b) Schematic of Stokes shift between absorption and emission, reproduced from Sobarwiki [23]. (c) Absorption (black line) and emission (red line) spectra of tetracene in solution, demonstrating the Frank-Condon principle. Reprinted from Burdett *et al.* [24], with the permission of AIP Publishing. (d) Absorption and emission spectra of P3HT aggregates in solution and spin coated at -80°C . Features in the film are broadened with respect to the solution. Reprinted with permission from Ferreira *et al.* [25]. Copyright 2012 American Chemical Society. (e) Absorbance (dotted) and photoluminescence (solid line) of exfoliated 2D halide perovskites, BA₂MA_{n-1}Pb_nI_{3n+1}, where BA is *n*-butylamine, MA is methylammonium, and *n* is the number of metal-halide sheets (number defined in plot). Reprinted (adapted) with permission from Paritmongkol *et al.* [26]. Copyright 2019 American Chemical Society.

phonons); defects; and intrinsic and extrinsic material properties, including diffusion lengths, sample thickness, and surface roughness (which can all broaden photoluminescence) [32–34]. While photoluminescence is straightforward to model in some materials [35–37], typically, it is more complicated to theoretically model than absorption coefficients. For example, crystal lattice deformation goes beyond the Born-Oppenheimer approximation, preventing the direct application of density functional theory and similar approaches [38]. We note that Huang-Rhys theory has been successful in modeling the photoluminescence of several organic molecule based semiconductors [39].

The energy difference between the band gap and PL peak [40], termed the Stokes shift [Fig. 2(b)], is a clear indicator of the amount of energy lost before radiative emission can occur. Materials with small Stokes shifts (and thus, significant overlap between absorption and emission spectra), for example, III-V semiconductors, some

single-walled carbon nanotubes, and halide perovskites [41–43], will have significant amounts of photon reabsorption, where many emitted photons cannot escape the material. Alternatively, materials with large Stokes shifts (or those that form self-trapped excitons) indicate significant energy loss, which can be attributed to several processes that correspond to concurrent energy loss to phonons alongside photon emission [40,44]. In some materials, PL can be observed at higher energies than the band gap. PL at slightly higher energies than the band gap suggests misinterpretation of the band gap due to strong sub-band-gap absorption (typically from defects)—here further measurements of sub-band-gap absorption (e.g., via photothermal deflection spectroscopy [45,46]) may be necessary. PL peaks being significantly higher than absorption can be caused by a range of upconversion processes [47,48]—to confirm if this is the case, photoluminescence should be recorded while the sample is excited close to its band gap.

IV. ABSORPTION AND PHOTOLUMINESCENCE SHAPE

A transition from a filled to an empty energy level (the basis of both absorption and photoluminescence) results in destruction or creation of a photon at a specific energy. However, absorption and photoluminescence spectra are broad continuous features—this is due to “smearing” of individual energy levels caused by hybridization into bands and temperature broadening, among other contributions [49]. The resulting shape of absorption and photoluminescence signals can be difficult to interpret, with low temperature measurements, where broadening effects can be reduced, often able to reveal key features [50].

If vibronic transitions have similar energies to optical transition energies, then these processes can couple. This is seen most prominently in small organic molecules. The coupling can result in splitting of absorption and photoluminescence spectra into several peaks, corresponding to different orders of vibronic transition. In this case, absorption and photoluminescence spectra are (ideally) mirror images of each other, following the Franck-Condon principle, as presented in Fig. 2(c) for tetracene in solution. Therefore, if this is observed, it is strongly suggestive of vibronic transitions being important in the system. However, in thin films, peaks can often be smeared out via sample impurities or heterogeneity over several micrometers, as shown for the organic molecule poly(3-hexylthiophene-2,5-diyl) (P3HT) in Fig. 2(d), so it is not always possible to definitively assign vibronic coupling without temperature-dependent measurements (where the population of different vibronic states can be modulated) [39]. Notably, in this case, photoluminescence peaks at several energies can be seen. The opposite—broad absorption spectra but a single photoluminescence peak—is observed when all excitations rapidly fall to the lowest energy level following excitation. This is the case in most inorganic semiconductors at room temperature (e.g., silicon, GaAs) and is presented in Fig. 2(e) for 2D halide perovskites. An important additional feature for these 2D halide perovskites, which have strong exciton binding energies, is that each absorption spectrum has a strong peak close to the band gap. This peak exists in all direct-band-gap semiconductors (though is often extremely weak) and is typically interpreted as an exciton resonance near the band gap at a specific energy (while higher-energy absorption rapidly results in free charge formation) [51]. Exciton resonances can be modeled via the Bethe-Salpeter approach to simulating excited states [52].

V. PLQE

PLQE quantifies the number of photons emitted relative to those absorbed [8]. It is the combination of two measurements recorded at the same time: sample absorption at an excitation wavelength and photoluminescence.

PLQE is typically recorded with an incident beam wider than 10 μm so carrier diffusion in samples can be ignored. Wavelength and spectral response calibration are again necessary, while absolute quantification of the number of photons incident on the sample can be achieved via appropriate use of a power meter. We note that relative PLQE measurements (i.e., the relative intensity of two signals) also carry significant information and do not require absolute photon quantification. Ideally, repeated measurements of samples should be carried out to avoid any errors due to poor sample loading or alignment. If possible, PLQE should be measured for each PL peak separately. We note that PLQE can be very sensitive to incident laser intensity, and so, excitation irradiance should always be stated alongside any reported measurement. PLQE can also be recorded following pulsed laser excitation, but it is important to highlight that, in this case, the signal is an integral over a transient decay, rather than a steady-state measurement constant in time.

If PLQE is near 100%, then radiative recombination is dominant in the material, and there are few other loss pathways available to excitations. We note that a sample with high PLQE can still have a high Stokes shift, so 100% PLQE does not imply there is no energy loss, just a high conversion of photons in into photons out. Measured PLQE is typically referenced to as the external PLQE, $\eta_{\text{PLQE,ext}}$. In materials with small Stokes shifts, photon reabsorption can have a significant effect. Here, the probability that an excited species emits a photon, the internal PLQE, $\eta_{\text{PLQE,int}}$, can be orders of magnitude higher than the external PLQE. The precise relationship is

$$\eta_{\text{PLQE,int}} = \frac{\eta_{\text{PLQE,ext}}}{\eta_{\text{esc}} + (1 - \eta_{\text{esc}})\eta_{\text{PLQE,ext}}},$$

where η_{esc} is the probability that an emitted photon escapes the material [53]. We briefly note that η_{esc} relates properties including the sample’s surface roughness and substrate properties, meaning $\eta_{\text{PLQE,ext}}$ is not an intrinsic material property.

When a sample is deposited on a substrate, its two surfaces are exposed to different surroundings. The PLQE may change significantly when the sample is excited from either the front or back sides, indicating that one surface has significantly more traps present, as shown to be the case in CdTe [54], for example. This can be further explored by measuring PLQE at different excitation wavelengths, as longer wavelengths will typically have greater absorption depths, and thus, will generate more excitations further from the surfaces. The two surfaces having very different characters mean that it is unlikely for a uniform excitation density to be built up following photoexcitation. This, in turn, implies that TRPL fitting should not be carried out for these samples, beyond first-order fitting (see Sec. VI). Finally, we note that the PL shape should be

identical for front and back illumination if the sample has a large Stokes shift (so no photon reabsorption occurs [53]), similar densities of charge traps on both surfaces, or totally uniform excitation from the front to the back of the film (assuming there is no compositional gradient throughout the film, which can occur, for example, in copper indium gallium selenide materials [55]).

The most useful information that can be gained from PLQE is when it is recorded at multiple excitation powers. First, the absorbance of stable samples should be constant at all excitation powers. Indeed, changes in absorbance are a simple and direct measure of sample stability during measurement. Even if the absorbance does not change with excitation power, it is sensible to record PLQE from low to high power and then take a low-power measurement at the end of all other measurements to check for any hysteretic effects, for example, those induced by changes to the sample after illumination.

PLQE corresponds to the radiative recombination rate divided by the total recombination rate (as absorbed laser power must be equal to the total recombination rate). For excitons, radiative recombination is a first-order process, while for weakly doped free charge systems it is a second-order process at all excitation densities (and for strongly doped systems, it is a second-order process at high excitation densities). Other loss processes can be first, second, or third order in both cases (see the Supplemental Material Note 1 for further discussion [10]). Therefore, by measuring PLQE as a function of laser power, the form of the PLQE with laser power gives significant information on the recombination. We summarize the behavior for different systems in Fig. 3 (see Supplemental Material Note 3 for a model description [10]), though we note that laser powers available often prevent the whole of this curve from being recorded in experiments. For systems in which the dominant species are free charges, when moving from very low to very high laser powers, the PLQE should increase to a maximum (where second-order recombination is maximized and trap states are saturated) and then decrease as third-order (e.g., Auger) processes start to dominate. By contrast, for systems with bound charges (excitons), PLQE should be flat or decrease as the laser power is increased until a point where second-order (e.g., exciton-exciton) effects dominate. More generally, it is always correct to say that if PLQE increases/remains constant/decreases with laser power then the radiative rate is a higher/same/lower order process than the nonradiative process at these excitation densities. It is also possible to fit these PLQE data to extract ratios of key decay rate parameters, as we have recently done [56]. Finally, we note that if the PLQE of two PL peaks change in different ways with laser power, this shows that these PL peaks are governed by different recombination processes.

Following the steady-state measurements outlined above, the following properties can be understood: the

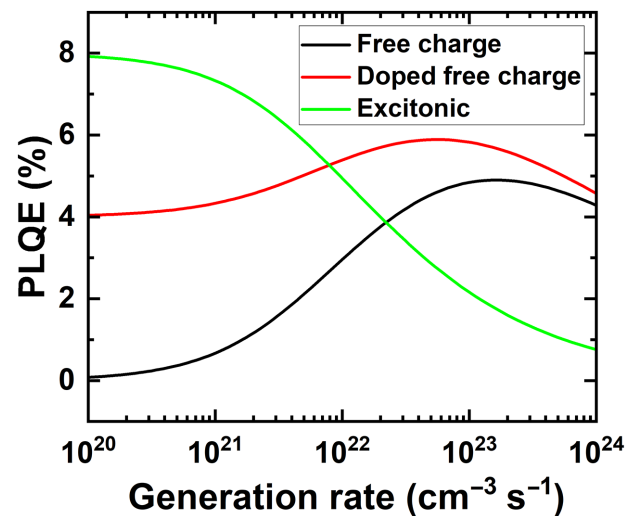


FIG. 3. Modeled photoluminescence quantum efficiency curves, as a function of the excitation rate per unit volume per unit time, for an undoped system with free charges, for a doped system with free charges, and for an excitonic system. Modeling assumptions can be found in the Supplemental Material Note 3 [10].

material band gap, energy loss prior to photoluminescence, the role of surfaces, material stability, hysteresis in intensity-dependent measurements, whether all PL peaks are governed by the same recombination processes, whether recombination is governed by free charges or excitons (via scaling of PLQE with laser power), and the relative strength and order of radiative and nonradiative rates. However, uncertainty will remain around what exactly is occurring between absorption and recombination, for example, do charges significantly diffuse through the material, whether charge trapping is a rapid process that competes with radiative recombination, or what the excited state lifetime is within the material. TRPL can begin to answer these questions.

VI. TRPL

Several approaches can be used to record TRPL, including time-correlated single photon counting (TCSPC) via single-photon avalanche diodes (SPADs), streak cameras, and intensified charge coupled devices (ICCD) [9,57,58]. The basic principle is the same in all cases: a laser pulse excites the sample and PL is recorded as a function of time following excitation. From a physical point of view, the key difference between different measurements is the time between laser pulses—in TCSPC, only a single photon is recorded after each laser pulse, meaning pulses are typically spaced closer (~ 10 ns- 10 μ s between pulses) than in streak cameras or ICCD (~ 1 ms between pulses). This means TCSPC can give different results to streak cameras or ICCD in samples where charge traps (though not the

TRPL) live longer than the time between pulses, which we elaborate on below. TCSPC is also more sensitive to lower signal levels, making it useful for studying luminescence from defects. For full analyses, TRPL should be recorded at all PL peaks, giving a second method (alongside PLQE with power) to ascertain if the same recombination processes govern all peaks. Furthermore, for a new material, TRPL should be recorded at several different timescales (ideally from ps to μ s), in case there are fast and slow recombination components. When choosing which equipment should be used to measure TRPL, spectral, temporal, and brightness limitations should be accounted for; these are listed in detector manuals.

In the discussion below, we assume that absorption and PL measurements of the sample have already been recorded, allowing a TRPL measurement to be well planned. The first useful information from TRPL measurements is an indication of the lifetime of optically active excited states. Fitting a mathematical model to the decay inherently assumes a physical model. It is tempting to adopt a model to fit data and assume it is correct because it mathematically “fits,” but any model must be physically validated and sensible before key information can be extracted. For example, use of biexponential decays can imply two separate first-order processes (e.g., surface and bulk recombination), but can also lead to significant misinterpretation of results in new systems, for example, fitting of second-order processes with two first-order curves would be incorrect. On the other hand, most halide perovskite systems can be fitted by first-, second-, and third-order decay rates with reasonable physical justifications [59]. Simpler methods can give a rough indication of lifetimes and allow for rapid comparison between samples, even without knowledge of a model or underlying

recombination processes e.g., the time for the initial signal to fall to $1/e$. However, we note that this time (and any lifetime) is often a function of the excitation density, as presented in Fig. 4(a). Therefore, when quoting this value, the incident pump irradiance, duration, and repetition rate must be reported side by side, though, in general, fluence-dependent measurements are more appropriate to obtain a full system understanding (see below). Key to any operating device is the trade-off between excited charge lifetime and diffusion rate. Therefore, when optimizing a material, longer lifetimes at low fluence (i.e., in a trap-dominated regime), in general, are an improvement, but care should be taken when comparing values between different materials.

In any TRPL measurement, signals should be recorded at several excitation powers and temporally offset to allow for decay overlays [as in Fig. 4(b), noting that statistical models should be applied to confirm the overlay in the case where data are unclear]. If these decays fully overlay, then excitations reach a consistent distribution from the front to the back of the film almost immediately following photoexcitation, and populating charge traps is not a dominant process at early times. However, it is more common to see the situation in Fig. 4(b), where a history-dependent part follows each excitation. This can be explained by noting that, immediately following photoexcitation, excited charges follow a Beer-Lambert-type distribution from the front to the back of the film. Excited charges will then both populate trap states and diffuse to a different distribution from the front to the back of the film. The history-dependent signal originates from before charge redistribution is complete. While some insight into charge redistribution can be gained on trapping and/or diffusion by carrying out measurements at different excitation wavelengths (e.g., to vary the initial charge distribution in the

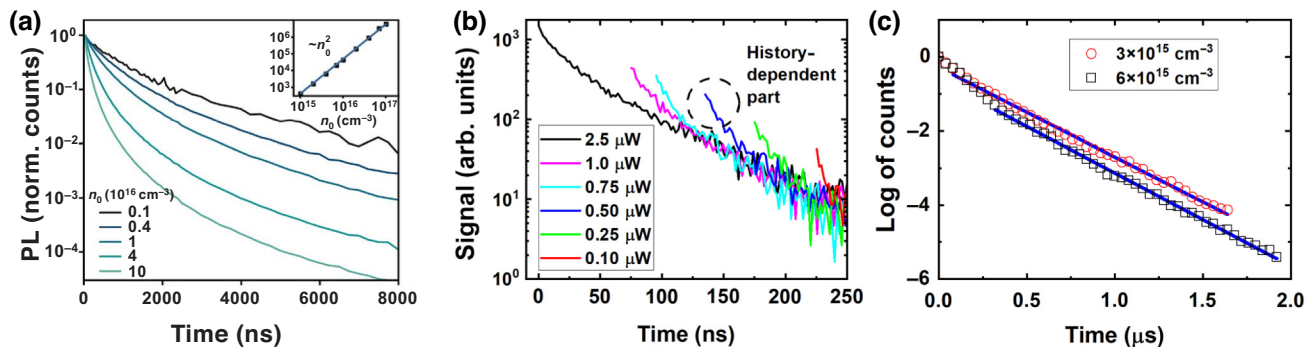


FIG. 4. (a) Normalized TRPL decays for a MAPbI₃ film at different excitation densities. Time for the decay to fall to $1/e$ of its initial value depends on the excitation density (see legend for excitation densities). Reproduced from Nagane *et al.* [59] (b) TCSPC signals of a formamidinium-cesium lead iodide (Cs_{0.3}FA_{0.7}PbI₃) halide perovskite following excitation at 470 nm at different incident laser powers (see legend), with signals offset from each other in time. Initial history-dependent part can be seen in signals. Cs_{0.3}FA_{0.7}PbI₃ samples are supplied by Rohit Prasana following standard preparation methods [60], and TCSPC measurements follow methods previously described [61]. (c) Fitting of decay rates on a log-lin plot (for two initial excitation densities), reprinted figure with permission from Bowman *et al.* [56]. Copyright 2022 by the American Physical Society.

film) or on materials already well spectroscopically characterized [62], it is challenging to unambiguously disentangle all competing contributions in the history-dependent part, often preventing a full fitting of TRPL data, unless this initial drop is negligible. Therefore, for new materials, we recommend analyzing the history-independent part, as discussed below.

Different communities approach fitting TRPL signals via qualitative or derived models. Fully qualitative models are appealing, but often lead to misinterpretation of results, unless a significant volume of data are fitted by several competing models and chi-square testing is carried out to compare models. Common processes that can happen to an excitation are trap-assisted surface recombination, trap-assisted bulk recombination, radiative recombination, and nonradiative multicarrier processes [e.g., Auger recombination of one (two) excited electron(s) and two (one) excited hole(s)] [11,63]. Several reviews already exist on full theoretical models [12], and we present typical descriptions and common simplifications for bound and free excitations in the Supplemental Material Note 1 [10]. The key point we highlight here is that, unless the history-dependent part of a TRPL decay is minimal, only first-order decay rates can be applied to fit TRPL curves with any degree of certainty. This is because all higher-order decay models require an estimate of the excitation density. While initial excitation density can be estimated immediately following photoexcitation (assuming that the laser pulse is sufficiently short that recombination processes are negligible for its duration), the history-dependent part of the decay, where charges have not redistributed throughout a material, is (for a new material) difficult to model. Therefore, it is not possible to know the excitation distribution following this history-dependent part, where charges redistribute (for an example of redistribution, see O'Hara *et al.* [64]). The two exceptions to this are when almost no photon reabsorption occurs—in materials with large Stokes shifts, or that are extremely thin—then the TRPL signal is directly proportional to the excitation density, with the same scaling factor at all times. Except in these special cases, we recommend only fitting history-independent parts of TRPL decay curves, where a straight line is observed on a log-lin plot, as in Fig. 4(c). This is because only straight lines on log-lin plots do not require an estimate of carrier density (see the Supplemental Material Note 4 [10]). We note that the same first-order decay rate will be obtained from TCSPC, ICCD, and streak cameras independent of laser pulse repetition rate (though for experimental rigor, multiple laser repetition rates should be explored and be low enough to ensure the background is accurately recorded [65,66]). One additional complexity exists when fitting an exponential decay, e^{-at} (where a is the first-order decay rate and t is time): for bound excitations, TRPL is proportional to the number of excitations. However, for free charges, TRPL is proportional

to the product of the number of excited electrons and holes. This means, for excitonic materials, a is the total first-order decay rate, while, for weakly doped free charge materials, $a/2$ is the first-order decay rate. In most luminescent semiconductors, the first-order decay rate can be directly associated with a charge trapping lifetime (see the Supplemental Material Note 1 [10]).

If the material has a minimal history-dependent part of the TRPL decay, then higher-order rates can be extracted, as excitation density can be estimated [59]. To estimate excitation density, the beam shape, sample thickness, and sample absorbance must be measured. We note that Gaussian beam shapes can result in significantly different values compared to the frequently assumed top hat beam shape [56]. To carry out these fittings, ideally, no excitations should be present from the previous laser pulse (including long-lived traps, see below), meaning second- and third-order rates should be extracted only at very low repetition rates. Otherwise, the estimated excitation density is lower than the “true” excitation density in the film. Due to these complexities and material requirements, second- and third-order recombination rates have much wider uncertainties associated with them, with most results not being reproducible [62,63,67].

Using appropriate measurement conditions (setting measurement bins to very short times), it is possible to observe the TRPL signal immediately following photoexcitation (prior to a history-dependent drop), termed $S_{\text{TRPL},0}$. How this quantity scales with excitation power provides key information: if $S_{\text{TRPL},0} \propto P_L$, where P_L is the laser power, this is indicative of the initial photoluminescence being from either excitons or strongly doped semiconductors [where a free electron (hole) recombines with a background hole (electron)]. Alternatively, if $S_{\text{TRPL},0} \propto P_L^2$, this shows the initial PL is due to free charges recombining. Examples of free charge (MAPbI₃) and excitonic (platinum octaethylporphyrin, PtOEP, an organic crystal [68]) systems are presented in Fig. 5(a). Contributions of both first- and second-order signals suggests a doped semiconductor. When using TCSPC, the repetition rate should be set to as long as possible, while still enabling the time 0 signal to be recorded (noting the full decay does not need to be recorded), as otherwise charges from the previous laser pulse can also contribute to the signal, as shown in Fig. 5(b) and 5(c). Here, as the time between pulses is lengthened, $S_{\text{TRPL},0}$ decreases, despite the fact that the TRPL signal is within noise prior to the subsequent laser pulse. This is due to excitations (e.g., holes) lasting a long time in trap states and only slowly recombining with free electrons that continue to be present in the system. These free electrons can also interact with newly excited holes from the subsequent laser pulse, contributing to $S_{\text{TRPL},0}$. In fact, the length of time between pulses above which $S_{\text{TRPL},0}$ is constant gives key information about the lifetime of nonradiative species present in a semiconductor. In the

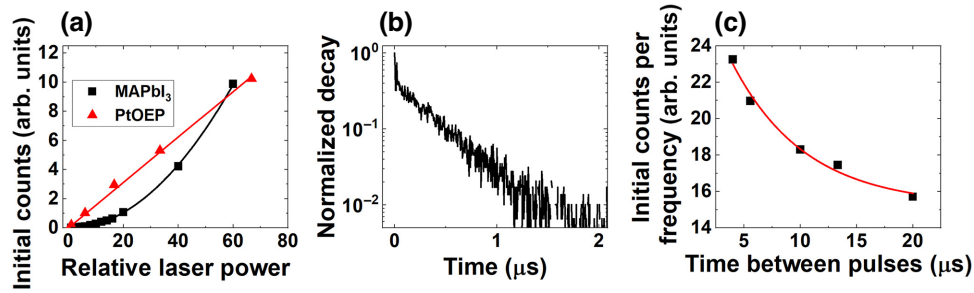


FIG. 5. (a) Scaling of initial TRPL counts for a free-charge (MAPbI₃) system with low doping and an excitonic system (PtOEP). Fits are quadratic and linear, respectively. Data are generated via ICCD using the setup we previously described. [56] (b) Typical recorded TCSPC decay, where the signal falls to the instrument background level (5 μs between laser pulses). (c) Scaling of initial counts per laser frequency of this signal (proportional to $S_{\text{TRPL},0}$), as a function of the time between incident laser pulses. It can be seen that $S_{\text{TRPL},0}$ continues to reduce even when the time between pulses is much longer than the decay time, due to charge traps continuing to be occupied. Data for (b),(c) are generated using a 520 nm laser (PicoQuant LDH 400) pulse and recorded by a single-photon avalanche diode (LifeSpec – ps, Edinburgh Instruments). PtOEP is deposited on glass sonicated in isopropyl alcohol and then acetone via evaporation at a pressure of 10^{-5} mbar and temperature of 205 °C using an evaporation rate of about 0.2 \AA s^{-1} to achieve a thickness of approximately 10 nm. MAPbI₃ samples in (b),(c) are prepared following Nagane *et al.* [59].

limit of a long time between excitation pulses, the $S_{\text{TRPL},0}$ signal can be used to estimate the doping level within a free charge like material [56].

While TRPL measurements often carry convoluted information, they can be used to quantify charge lifetimes; doping levels; an indication of the timescale for charges to reach a steady-state distribution from the front to the back of the film; the lifetime of nonradiative species (via varying repetition rates) in the material; and, in some cases, higher-order decay rates [59]. TRPL can also be combined with PLQE to estimate absolute values for higher-order decay rates [56]. TRPL can be especially useful when comparing different passivation approaches to a material, as it offers a quick and easy way to measure the lifetime of excited charges (though care should be noted for the fluence-dependent nature of lifetime, as discussed earlier). At this point, an experimenter should have a good idea of the nature of excitations in their material and be able to identify the key loss processes occurring.

VII. TRANSLATION TO DEVICES

All methods described above should be applied to bare samples, with a higher-quality material resulting in a better device. However, the quality of charge extraction and how surface trapping rates change in devices due to charge extraction are missed when studying bare films. In general, it is not straightforward to ascertain this information from purely optical measurements, and instead these should be coupled to electronic measurements [69]. For example, one can extract these parameters via photoconductivity. We note that variables including mobility can also be extracted through a variety of contact (e.g., field-effect transistor

[70]) and contactless (e.g., terahertz spectroscopy [71]) measurements. Discussion of such approaches and parameters are beyond the scope of this work but should be explored for the complete characterization of a semiconductor. We also note that this is an active area of research and a comprehensive approach that can be applied to any device has not yet been realized [72].

Photoluminescence and TRPL can be observed from full devices or bilayers. High PLQEs and long TRPL lifetimes can be indicative of both good and bad devices. In an ideal solar cell, the charge extraction layers should not quench the PL when the device is at its open-circuit voltage (V_{OC}), and so, the PL should be identical in a thin film or a device. Any quenching of the PL at open circuit implies carriers now have additional nonradiative recombination pathways, causing quasi-Fermi level splitting (and corresponding V_{OC}) to be reduced [69]. However, in non-ideal devices, PL may be quenched due to charges being rapidly extracted to (nonideal) charge extraction layers. At the maximum power point, PL should be substantially quenched (in both ideal and nonideal situations), as the majority of carriers are now extracted rather than radiatively recombining in the active layer. In this case, the electroluminescence (EL) of the device would also be efficient. If the PL is not quenched at biases below V_{OC} , it implies carriers are not being efficiently extracted and, conversely, that charges will not be efficiently injected, and so, the EL in this case will not be efficient. As such, care should be taken when interpreting PL intensities of device stacks at V_{OC} without the addition of voltage-dependent PL and EL data. The approaches we outline above allow for an understanding of the material to be gained, which is necessary before full devices are analyzed and optimized.

VIII. CONCLUSION

Here, we provide focused guidelines to understand new luminescent semiconductors, with unknown photophysical properties, using simple spectroscopic measurements. We identify the wide range of information that can be extracted using these approaches and showcase a variety of results from different semiconductors. Finally, we briefly comment on applying these tools to full devices. These approaches will help to streamline the development, understanding, and optimization of future semiconductors for a variety of device applications.

ACKNOWLEDGMENTS

The authors thank the Engineering and Physical Research Sciences Council (EPSRC) for funding through an institutional award and Grant No. EP/R023980/1. The authors acknowledge support from the European Research Council (ERC, European Union's Horizon 2020, HYPERION 756962). S.D.S. acknowledges funding from the Royal Society and Tata Group (Grant No. UF150033). A.R.B. thanks Kyle Frohna, Simon Kahmann, Daniel Sowood, Tomi Baikie, Jacob Lever, and Bernd Sturza for their helpful suggestions when preparing this work.

-
- [1] Z.-K. Tan, R. S. Mghaddam, M. L. Lai, P. Docampo, R. Higler, F. Deschler, M. Price, A. Sadhanala, L. M. Pazos, D. Credgington, F. Hanusch, T. Bein, H. J. Snaith, and R. H. Friend, Bright light-emitting diodes based on organometal halide perovskite, *Nat. Nanotechnol.* **9**, 687 (2014).
- [2] Y. Zhou, J. Chen, O. M. Bakr, and O. F. Mohammed, Metal halide perovskites for x-ray imaging scintillators and detectors, *ACS Energy Lett.* **6**, 739 (2021).
- [3] L. J. Phillips, C. N. Savory, O. S. Hutter, P. J. Yates, H. Shiel, S. Mariotti, L. Bowen, M. Birkett, K. Durose, D. O. Scanlon, and J. D. Major, Current enhancement via a TiO₂ window layer for CSS Sb₂Se₃ solar cells: Performance limits and high V_{OC} , *IEEE J. Photovoltaics* **9**, 544 (2019).
- [4] M. A. Green, A. Ho-Baillie, and H. J. Snaith, The emergence of perovskite solar cells, *Nat. Photonics* **8**, 506 (2014).
- [5] L. C. Lee, T. N. Huq, J. L. Macmanus-Driscoll, and R. L. Z. Hoyer, Research update: Bismuth-based perovskite-inspired photovoltaic materials, *APL Mater.* **6**, 084502 (2018).
- [6] L. Zhu, *et al.*, Single-junction organic solar cells with over 19% efficiency enabled by a refined double-fibril network morphology, *Nat. Mater.* **21**, 656 (2022).
- [7] G. D. Gilliland, Photoluminescence spectroscopy of crystalline semiconductors, *Mater. Sci. Eng., R* **18**, 99 (1997).
- [8] J. C. De Mello, H. F. Wittmann, and R. H. Friend, An improved experimental determination of external photoluminescence quantum efficiency, *Adv. Mater.* **9**, 230 (1997).
- [9] D. Phillips, A lifetime in photochemistry; some ultrafast measurements on singlet states, *Proc. R. Soc. A* **472**, 4 (2016).
- [10] See the Supplemental Material at <http://link.aps.org/supplemental/10.1103/PRXEnergy.2.022001> for (i) a table outlining the main recombination models used, (ii) further discussion of Tauc fitting, (iii) explanation of PL quantum yield modeling, and (iv) discussion of estimating carrier density.
- [11] J. Nelson, *The Physics of Solar Cells* (Imperial College Press, London, 2003).
- [12] T. Kirchartz, J. A. Márquez, M. Stolterfoht, and T. Unold, Photoluminescence-based characterization of halide perovskites for photovoltaics, *Adv. Energy Mater.* **10**, 1904134 (2020).
- [13] Peter Würfel, *Physics of Solar Cells: From Principles to New Concepts* (Wiley, Hoboken, 2005).
- [14] Z. Chen, H. N. Dinh, and E. Miller, in *Photoelectrochemical Water Splitting: Standards, Experimental Methods, and Protocols*, edited by Z. Chen, H. N. Dinh, E. Miller (Springer New York, New York, NY, 2013), pp. 49–62.
- [15] E. Yablonovitch, Statistical ray optics, *J. Opt. Soc. Am.* **72**, 899 (1982).
- [16] J. M. Ball, S. D. Stranks, M. T. Hörantner, S. Hüttner, W. Zhang, E. J. W. Crossland, I. Ramirez, M. Riede, M. B. Johnston, R. H. Friend and H. J. Snaith, Optical properties and limiting photocurrent of thin-film perovskite solar cells, *Energy Environ. Sci.* **8**, 602 (2015).
- [17] F. Stern, *Solid State Physics* (Academic Press Inc., New York and London, 1963).
- [18] M. Rohlfing and S. G. Louie, Electron-hole excitations and optical spectra from first principles, *Phys. Rev. B* **62**, 1 (2000).
- [19] J. Tauc, Optical properties and electronic structure of amorphous Ge and Si, *Mater. Res. Bull.* **3**, 37 (1968).
- [20] K. Papatryfonos, T. Angelova, A. Brimont, B. Reid, S. Guldin, P. R. Smith, M. Tang, K. Li, A. J. Seeds, H. Liu, and D. R. Selviah, Refractive indices of MBE-grown Al_xGa_(1-x) as ternary alloys in the transparent wavelength region, *AIP Adv.* **11**, 025327 (2021).
- [21] M. A. Green, Self-consistent optical parameters of intrinsic silicon at 300 K including temperature coefficients, *Sol. Energy Mater. Sol. Cells* **92**, 1305 (2008).
- [22] A. R. Bowman, F. Lang, Y.-H. Chiang, A. Jiménez-Solano, K. Frohna, G. E. Eperon, E. Ruggeri, M. Abdi-Jalebi, M. Anaya, B. V. Lotsch, and S. D. Stranks, Relaxed current matching requirements in highly luminescent perovskite tandem solar cells and their fundamental efficiency limits, *ACS Energy Lett.* **6**, 612 (2021).
- [23] Sobarwiki, Stokes Shift, <https://commons.wikimedia.org/w/index.php?curid=29474504>
- [24] J. J. Burdett, A. M. Müller, D. Gosztola, and C. J. Bardeen, Excited state dynamics in solid and monomeric tetracene: The roles of superradiance and exciton fission, *J. Chem. Phys.* **133**, 144506 (2010).
- [25] B. Ferreira, P. F. da Silva, J. S., Seixas de Melo, J. Pina, and A. Maçanita, Excited-state dynamics and self-organization of poly(3-hexylthiophene) (P3HT) in solution and thin films, *J. Phys. Chem. B* **116**, 2347 (2012).
- [26] W. Paritmongkol, N. S. Dahod, A. Stollmann, N. Mao, C. Settens, S.-L. Zheng, and W. A. Tisdale, Synthetic variation and structural trends in layered two-dimensional alkylammonium lead halide perovskites, *Chem. Mater.* **31**, 5592 (2019).

- [27] M. Ledinsky, T. Schönfeldová, J. Holovský, E. Aydin, Z. Hájková, L. Landová, N. Neyková, A. Fejfar, and S. De Wolf, Temperature dependence of the Urbach energy in lead iodide perovskites, *J. Phys. Chem. Lett.* **10**, 1368 (2019).
- [28] D. Marongiu, M. Saba, F. Quochi, A. Mura, and G. Bongiovanni, The role of excitons in 3D and 2D lead halide perovskites, *J. Mater. Chem. C* **7**, 12006 (2019).
- [29] B. D. Viezbicke, S. Patel, B. E. Davis, and D. P. Birnie, Evaluation of the Tauc method for optical absorption edge determination: ZnO thin films as a model system: Tauc method for optical absorption edge determination, *Phys. Status Solidi B* **252**, 1700 (2015).
- [30] Z. Wang, Q. Lin, F. P. Chmiel, N. Sakai, L. M. Herz, and H. J. Snaith, Efficient ambient-air-stable solar cells with 2D–3D heterostructured butylammonium-caesium-formamidinium lead halide perovskites, *Nat. Energy* **6**, 17135 (2017).
- [31] NIST: Atomic Spectra Database Lines Form, https://physics.nist.gov/PhysRefData/ASD/lines_form.html.
- [32] G. Lanzani, *The Photophysics behind Photovoltaics and Photonics* (John Wiley & Sons, Ltd, Weinheim, Germany, 2012).
- [33] C. Wehrenfennig, M. Liu, H. J. Snaith, M. B. Johnston, and L. M. Herz, Homogeneous emission line broadening in the organo lead halide perovskite $\text{CH}_3\text{NH}_3\text{PbI}_{3-x}\text{Cl}_x$, *J. Phys. Chem. Lett.* **5**, 1300 (2014).
- [34] R. B. Capaz, C. D. Spataru, P. Tangney, M. L. Cohen, and S. G. Louie, Temperature Dependence of the Band Gap of Semiconducting Carbon Nanotubes, *Phys. Rev. Lett.* **94**, 036801 (2005).
- [35] L. M. Pazos-Outón, T. P. Xiao, and E. Yablonovitch, Fundamental efficiency limit of lead iodide perovskite solar cells, *J. Phys. Chem. Lett.* **9**, 1703 (2018).
- [36] E. T. Niles, J. D. Roehling, H. Yamagata, A. J. Wise, F. C. Spano, A. J. Moulé, and J. K. Grey, *J*-Aggregate behavior in poly-3-hexylthiophene nanofibers, *J. Phys. Chem. Lett.* **3**, 259 (2012).
- [37] F. C. Spano, Absorption in regio-regular poly(3-hexyl)thiophene thin films: Fermi resonances, interband coupling and disorder, *Chem. Phys.* **325**, 22 (2006).
- [38] F. Guistino, *Materials Modelling Using Density Functional Theory: Properties and Predictions* (Oxford University Press, Oxford, 2014).
- [39] L. Farouil, F. Alary, E. Bedel-Pereira, and J.-L. Heully, Revisiting the vibrational and optical properties of P3HT: A combined experimental and theoretical study, *J. Phys. Chem. A* **122**, 6532 (2018).
- [40] E. L. Mertz, V. A. Tikhomirov, and L. I. Krishtalik, Stokes shift as a tool for probing the solvent reorganization energy, *J. Phys. Chem. A* **101**, 3433 (1997).
- [41] J. E. Parrott, Radiative recombination and photon recycling in photovoltaic solar cells, *Sol. Energy Mater. Sol. Cells* **30**, 221 (1993).
- [42] A. Graf, Y. Zakharko, S. P. Schießl, C. Backes, M. Pfohl, B. S. Flavel, and J. Zaumseil, Large scale, selective dispersion of long single-walled carbon nanotubes with high photoluminescence quantum yield by shear force mixing, *Carbon* **105**, 593 (2016).
- [43] L. M. Pazos-Outon, M. Szumilo, R. Lamboll, J. M. Richter, M. Crespo-Quesada, M. Abdi-Jalebi, H. J. Beeson, M. Vrućinić, M. Alsari, H. J. Snaith, B. Ehrler, R. H. Friend, and F. Deschler, Photon recycling in lead iodide perovskite solar cells, *Science* **351**, 1430 (2016).
- [44] R. Kentsch, M. Morgenroth, M. Scholz, K. Xu, J. Schmedt auf der Günne, T. Lenzer, and K. Oum, Direct observation of the exciton self-trapping process in CsCu_2I_3 thin films, *J. Phys. Chem. Lett.* **11**, 4286 (2020).
- [45] S. Han, *et al.*, Lanthanide-doped inorganic nanoparticles turn molecular triplet excitons bright, *Nature* **587**, 594 (2020).
- [46] L. Goris, K. Haenen, M. Nesládek, P. Wagner, D. Vanderzande, L. De Schepper, J. D'haen, L. Luisen, and J. V. Manca, Absorption phenomena in organic thin films for solar cell applications investigated by photothermal deflection spectroscopy, *J. Mater. Sci.* **40**, 1413 (2005).
- [47] S. Balushev, V. Yakutkin, T. Miteva, Y. Avlasevich, S. Chernov, S. Aleshchenkov, G. Nelles, A. Cheprakov, A. Yasuda, K. Müllen, and G. Wegner, Blue-green up-conversion noncoherent excitation by NIR light, *Angew. Chem., Int. Ed.* **46**, 7693 (2007).
- [48] M. Haase and H. Schäfer, Upconverting nanoparticles, *Angew. Chem., Int. Ed.* **50**, 5808 (2011).
- [49] S. Kundu, P. P. Roy, G. R. Fleming, and N. Makri, Franck–Condon and Herzberg–Teller signatures in molecular absorption and emission spectra, *J. Phys. Chem. B* **126**, 2899 (2022).
- [50] T. Ito and T. Masumi, Detailed examination of relaxation processes of excitons in photoluminescence spectra of Cu_2O , *J. Phys. Soc. Jpn.* **66**, 2185 (1997).
- [51] Ye F. Gross, N. M. Reinov, Ye F. Gross, and N. M. Reinov, *Excitation in cuprous oxide crystals at the temperature of liquid helium (4.2°K)* (US Atomic Energy Commission, Technical Information Service, Ohio, USA, 1954), Vol. 185.
- [52] F. Fuchs, C. Rödl, A. Schleife, and F. Bechstedt, Efficient $O(N^2)$ approach to solve the Bethe-Salpeter equation for excitonic bound states, *Phys. Rev. B* **78**, 085103 (2008).
- [53] A. R. Bowman, M. Anaya, N. C. Greenham, and S. D. Stranks, Quantifying Photon Recycling in Solar Cells and Light-Emitting Diodes: Absorption and Emission Are Always Key, *Phys. Rev. Lett.* **125**, 067401 (2020).
- [54] J. D. Major, M. Al Turkestani, L. Bowen, M. Brossard, C. Li, P. Lagoudakis, S. J. Pennycook, L. J. Phillips, R. E. Treharne, and K. Durose, In-depth analysis of chloride treatments for thin-film CdTe solar cells, *Nat. Commun.* **7**, 13231 (2016).
- [55] T. Negami, T. Satoh, Y. Hashimoto, S. Shimakawa, S. Hayashi, M. Muro, H. Inoue, and M. Kitagawa, Production technology for CIGS thin film solar cells, *Thin Solid Films* **403–404**, 197 (2002).
- [56] A. R. Bowman, S. Macpherson, A. Abfalterer, K. Frohna, S. Nagane, and S. D. Stranks, Extracting Decay-Rate Ratios from Photoluminescence Quantum Efficiency Measurements in Optoelectronic Semiconductors, *Phys. Rev. Appl.* **17**, 044026 (2022).
- [57] M. Kögler and B. Heilala, Time-gated Raman spectroscopy – a review, *Meas. Sci. Technol.* **32**, 012002 (2020).
- [58] L. Cester, A. Lyons, M. C. Braidotti, and D. Faccio, Time-of-flight imaging at 10 ps resolution with an ICCD camera, *Sensors* **19**, 180 (2019).

- [59] S. Nagane, S. Macpherson, M. A. Hope, D. J. Kubicki, W. Li, S. D. Verma, J. F. Orri, Y.-H. Chiang, J. L. MacManus-Driscoll, C. P. Grey, and S. D. Stranks, Tetrafluoroborate-induced reduction in defect density in hybrid perovskites through halide management, *Adv. Mater.* **33**, 2102462 (2021).
- [60] R. Prasanna, A. Gold-Parker, T. Leijtens, B. Conings, A. Babayigit, H. G. Boyen, M. F. Toney, and M. D. McGehee, Band gap tuning via lattice contraction and octahedral tilting in perovskite materials for photovoltaics, *J. Am. Chem. Soc.* **139**, 11117 (2017).
- [61] A. R. Bowman, S. D. Stranks, and B. Monserrat, Investigation of singlet fission–halide perovskite interfaces, *Chem. Mater.* **34**, 4865 (2022).
- [62] M. J. Trimpl, A. D. Wright, K. Schutt, L. R. V. V. Buizza, Z. Wang, M. B. Johnston, H. J. Snaith, P. Müller-Buschbaum, and L. M. Herz, Charge-carrier trapping and radiative recombination in metal halide perovskite semiconductors, *Adv. Funct. Mater.* **30**, 2004312 (2020).
- [63] J. X. Shen, X. Zhang, S. Das, E. Kioupakis, and C. G. Van de Walle, Unexpectedly strong Auger recombination in halide perovskites, *Adv. Energy Mater.* **8**, 1801027 (2018).
- [64] K. E. O’Hara, J. R. Gullingsrud, and J. P. Wolfe, Auger decay of excitons in Cu_2O , *Phys. Rev. B* **60**, 10872 (1999).
- [65] A. Wappelt, A. Bergmann, A. Napiwotzki, H. J. Eichler, H. J. Jüpner, A. Kummrow, A. Lau, and S. Woggon, Picosecond time-resolved luminescence of tetracene thin films, *J. Appl. Phys.* **78**, 5192 (1995).
- [66] A. P. Herman, S. J. Zelewski, K. Misztal, and R. Kudrawiec, Probing the long-lived photo-generated charge carriers in transition metal dichalcogenides by time-resolved microwave photoconductivity, *Nanophotonics* **11**, 1335 (2022).
- [67] J. M. Richter, M. Abdi-Jalebi, A. Sadhanala, M. Tabachnyk, J. P. H. Rivett, L. M. Pazos-Outón, K. C. Gödel, M. Price, F. Deschler, and R. H. Friend, Enhancing photoluminescence yields in lead halide perovskites by photon recycling and light out-coupling, *Nat. Commun.* **7**, 13941 (2016).
- [68] T. Dienel, H. Proehl, T. Fritz, and K. Leo, Novel near-infrared photoluminescence from platinum(II)-porphyrin (PtOEP) aggregates, *J. Lumin.* **110**, 253 (2004).
- [69] M. Stolterfoht, C. M. Wolff, J. A. Márquez, S. Zhang, C. J. Hages, D. Rothhardt, S. Albrecht, P. L. Burn, P. Meredith, T. Unold, and D. Neher, Visualization and suppression of interfacial recombination for high-efficiency large-area *pin* perovskite solar cells, *Nat. Energy* **3**, 847 (2018).
- [70] S. P. Senanayak, B. Yang, T. H. Thomas, N. Giesbrecht, W. Huang, E. Gann, B. Nair, K. Goedel, S. Guha, X. Moya, C. R. McNeill, P. Docampo, A. Sadhanala, R. H. Friend, and H. Sirringhaus, Understanding charge transport in lead iodide perovskite thin-film field-effect transistors, *Sci. Adv.* **3**, 1 (2017).
- [71] R. L. Milot, G. E. Eperon, H. J. Snaith, M. B. Johnston, and L. M. Herz, Temperature-dependent charge-carrier dynamics in $\text{CH}_3\text{NH}_3\text{PbI}_3$ perovskite thin films, *Adv. Funct. Mater.* **25**, 6218 (2015).
- [72] L. Krückemeier, Z. Liu, B. Krogmeier, U. Rau, and T. Kirchartz, Consistent interpretation of electrical and optical transients in halide perovskite layers and solar cells, *Adv. Energy Mater.* **11**, 2102290 (2021).